European Congress on Computational Methods
in Applied Sciences and Engineering (ECCOMAS 2012)
J. Eberhardsteiner et.al. (eds.)
Vienna, Austria, September 10-14, 2012

FINITE STRAIN INELASTIC MODELS WITH GRADIENT AVERAGING AND ACEGEN IMPLEMENTATION

Balbina Wcisło[1], Tomasz Żebro[1], Katarzyna Kowalczyk-Gajewska[2] and Jerzy Pamin[1]

[1]Cracow University of Technology
Warszawska 24, 31-155 Kraków, Poland
e-mail: {bwcislo,tzebro,jpamin}@L5.pk.edu.pl

[2] Institute of Fundamental Technological Research of PAS
Pawińskiego 5B,02-106 Warszawa, Poland
e-mail: kkowalcz@ippt.gov.pl

Keywords: large strain, damage, plasticity, gradient-enhancement, AceGen package

Abstract. *This paper deals with the development of a family gradient-enhanced elasticity-damage-plasticity models for the simulation of failure in metallic and composite materials. The model incorporates finite deformations and is developed with the assumption of isotropy and isothermal conditions. The gradient enhancement applied to the damage part of the model aims at removing pathological sensitivity to the finite element discretization which can occur due to material softening.*

The attention is focused on the algorithmic aspects and on the implementation of the model using AceGen tool for automatic code generation, thus circumventing the cumbersome derivation of the consistent tangent for the Newton's method. Numerical verification tests of the described model are performed with the Mathematica-based package AceFEM. Particularly, uniaxial tension test for a bar with a variable cross-section and tension of a perforated plate are examined.

1 INTRODUCTION

The research presented in this paper is focused on the development of a family of gradient-enhanced elasticity-plasticity-damage models in large strain regime. The models can be used to reproduce the behaviour of metallic and composite materials.

A material model including damage involves a descending stress-strain branch (the post-peak regime). The material softening causes ill-posedness of the boundary value problem which results in pathological mesh-sensitivity in the numerical simulations. To obtain the material model which is capable to properly reproduce damage a gradient regularization is applied [6]. Moreover, taking into account finite deformations the problem becomes more difficult due to softening caused by the geometrical effects such as necking.

The paper is based on the concepts presented in papers [2], [1] and [5]. It includes a short presentation of the considered model, solution algorithm, AceGen/FEM implementation aspects [4] and selected results of computational tests. Finally, some conclusions and future work suggestions are gathered.

2 CONSTITUTIVE RELATIONS

The family of geometrically non-linear models presented in the paper is derived adopting the assumption of isotropy and isothermal conditions. The formulation is based on the multiplicative split of deformation gradient $\boldsymbol{F}$ into its elastic and plastic parts:

$$\boldsymbol{F} = \boldsymbol{F}^e \boldsymbol{F}^p \tag{1}$$

We employ the elastic left Cauchy-Green tensor

$$\boldsymbol{b}^e = \boldsymbol{F}^e \boldsymbol{F}^{eT} \tag{2}$$

which is considered in the work as the main internal variable.

The free energy function is assumed as an isotropic function of the elastic left Cauchy-Green tensor $\mathbf{b}^e$, a scalar measure of plastic flow γ and a scalar damage parameter ω:

$$\psi = (1-\omega)\psi^e(\mathbf{b}^e) + \psi^p(\gamma) \tag{3}$$

where the first term is associated with elasticity and damage and the second term with plasticity.

2.1 Hyperelasticity

The elastic part of the free energy ψ^e is a function of the elastic left Cauchy-Green tensor $\mathbf{b}^e$. Particularly, in the paper the free energy is decoupled into volumetric and deviatoric parts and formulated as follows [7]

$$\psi^e = \frac{\kappa}{2}\left[\frac{1}{2}(J_{be}-1) - \frac{1}{2}\ln(J_{be})\right] + \frac{\mu}{2}\left(\mathrm{tr}(J_{be}^{-1/3}\mathbf{b}^e) - 3\right) \tag{4}$$

where κ and μ are material parameters (respectively bulk and shear modulus) and J_{be} is the determinant of the elastic left Cauchy-Green tensor.
The relation between the Kirchhoff stress tensor $\boldsymbol{\tau}$ and the elastic left Cauchy-Green tensor $\mathbf{b}^e$ is nonlinear and can be derived from the free energy function in the form:

$$\boldsymbol{\tau} = 2\frac{\partial \psi^e}{\partial \mathbf{b}^e}\mathbf{b}^e \tag{5}$$

The Kirchhoff stress tensor can be split into its volumetric and deviatoric parts:

$$\boldsymbol{\tau} = p\boldsymbol{I} + \boldsymbol{t}, \qquad p = (\boldsymbol{\tau} : \boldsymbol{I})/3, \qquad \boldsymbol{t} = \boldsymbol{\tau} - p\boldsymbol{I} \tag{6}$$

2.2 Damage

When the scalar damage is added to the material description then the elastic free energy function is degraded and takes the form:

$$\psi^{e,d} = (1-\omega)\psi^{e} \tag{7}$$

The scalar damage variable ω grows from zero for the intact material to one for a complete material destruction and is computed from the damage growth function $\omega = f^{d}(\kappa)$, where $\kappa = \max(\tilde{\epsilon}, \kappa_0)$, $\tilde{\epsilon}$ is an equivalent strain or energy measure and κ_0 is the threshold. The damage evolution law can be formulated in different ways, see e.g. [3], and the formulation is tuned to the material of interest. In the following numerical simulations the exponential softening is assumed (Figure 1):

$$\omega(\kappa) = 1 - \frac{\kappa_0}{\kappa}\left(1 - \alpha + \alpha \exp(-\beta(\kappa - \kappa_0)\right) \tag{8}$$

where α and β are material parameters. The deformation measure which governs damage for materials undergoing large deformations is now assumed to be

$$\tilde{\epsilon} = \det(\boldsymbol{F}) - 1 \tag{9}$$

This definition implies that damage is directly connected with the increase of material volume. For incompressible materials or for simulations of sample compression damage will not occur. Other measures can be applied as well, for instance maximum eigenvalue of the left Cauchy-Green deformation tensor or elastic stored energy as in [8].
The damage condition takes the form:

$$F_d(\tilde{\epsilon}, \kappa) = \tilde{\epsilon} - \kappa \leq 0 \tag{10}$$

For $F_d < 0$ there is no growth of damage.

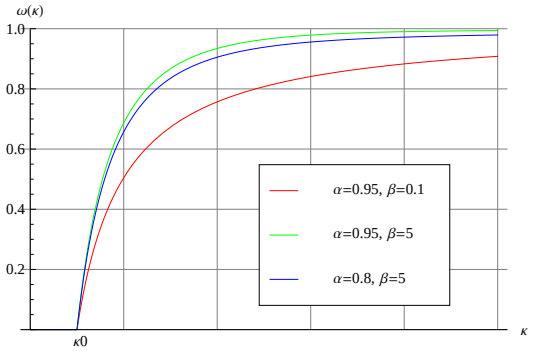

Figure 1: Exponential damage growth functions for different model parameters

2.3 Plasticity

In this section material damage is neglected in the constitutive relation. The plastic part of the free energy function is assumed in the form:

$$\psi^{p}(\gamma) = \frac{1}{2} h \gamma^{2} \tag{11}$$

where h is a material parameter identified with the hardening modulus. The plastic regime is defined through the yield function F_p which is an isotropic function of the Kirchhoff stress tensor $\boldsymbol{\tau}$ and the plastic multiplier γ:

$$F_p(\boldsymbol{\tau}, \gamma) = f(\boldsymbol{\tau}) - \sqrt{\frac{2}{3}}(\sigma_{y0} - q(\gamma)) \leq 0 \tag{12}$$

The function q can be derived from the plastic part of the free energy:

$$q(\gamma) = -\frac{d\psi^p(\gamma)}{d\gamma} \tag{13}$$

and represents the yield strength with for instance isotropic linear hardening: $q(\gamma) = -h\gamma$. The function f is assumed to be the Burzyński-Drucker-Prager plasticity function $f = \sqrt{2J_2} + \frac{\alpha_p}{3} I_1$, where α_p is a material constant, I_1 and J_2 are invariants of the effective Kirchhoff stress tensor:

$$I_1 = \boldsymbol{\tau} : \boldsymbol{I} \qquad J_2 = \frac{1}{2}\boldsymbol{t}^2 : \boldsymbol{I} \tag{14}$$

However, the solution algorithm is flexible and other yield criteria can easily be applied.
The associative flow rule is assumed in the form [2]:

$$-\frac{1}{2}\mathcal{L}_v \mathbf{b}^e = \dot{\gamma}\mathbf{N}\mathbf{b}^e \tag{15}$$

where $\mathcal{L}_v$ is the Lie derivative of $\mathbf{b}^e$ and $\mathbf{N}$ is a normal to the yield function:

$$\mathcal{L}_v \mathbf{b}^e = \mathbf{F}\frac{\partial}{\partial t}[(\mathbf{C}^p)^{-1}]\mathbf{F}^{\mathbf{T}} \qquad \mathbf{N} = \frac{\partial F}{\partial \boldsymbol{\tau}} \tag{16}$$

2.4 Elasticity-plasticity coupled with damage

In the paper an indirectly coupled model is considered, which means that the damage process is governed by the deformation measure and is not directly determined by the plastic flow. The plastic process is assumed to take place in the effective space, i.e. it governs the behaviour of the undamaged skeleton of the material. Consequently, the yield function depends on the effective Kirchhoff stress tensor $\hat{\boldsymbol{\tau}} = \boldsymbol{\tau}/(1-\omega)$ instead of $\boldsymbol{\tau}$ and has the form as in eq. (12):

$$F_p(\hat{\boldsymbol{\tau}}, \gamma) = f(\hat{\boldsymbol{\tau}}) - \sqrt{\frac{2}{3}}(\sigma_{y0} - q(\gamma)) \leq 0 \tag{17}$$

3 GRADIENT ENHANCEMENT

Higher-order gradient continuum theories are motivated by micro-defect interactions. In the gradient-enhanced damage model the local variable $\tilde{\epsilon}$ is substituted with its non-local counterpart $\bar{\epsilon}$ in damage condition (10). The non-local variable is specified by the averaging equation:

$$\bar{\epsilon} - l^2\nabla^2\bar{\epsilon} = \tilde{\epsilon} \tag{18}$$

with homogeneous natural boundary conditions. The parameter l appearing in equation (18) is a material-dependent length parameter commonly called the internal or intrinsic length scale. The Laplacian and the parameter l can be referred to either the deformed or the undeformed configuration [8] (these two cases are called in the paper material or spatial averaging). The gradient enhancement can prevent the numerical solution from pathological mesh-sensitivity.

4 SOLUTION ALGORITHM

In this section the solution algorithm for the gradient-enhanced elasticity-damage-plasticity model is described. From a computational point of view the nonlinear material behaviour is treated as configuration driven [2]. We wish to solve a nonlinear evolutionary problem over the time interval $[t_n, t_{n+1}]$, knowing the solution at time t_n, and current configuration (i.e. the deformation gradient). Particularly, from the previous time step the deformation gradient $\boldsymbol{F_n}$, the elastic part of the Cauchy-Green tensor $\boldsymbol{b}_n^e$, the plastic multiplier γ_n and the value of the damage history parameter κ_n are given. For the sake of brevity, all quantities related to the current time step t_{n+1} are written without indices. The coupled problem consists of the equilibrium and averaging equations to be solved.

Firstly, following [7], the relative deformation gradient is computed:

$$\boldsymbol{f} = \boldsymbol{F}\boldsymbol{F}_n^{-1} \tag{19}$$

Assuming that all the relative deformation gradient is elastic the trial elastic left Cauchy-Green tensor is calculated:

$$\boldsymbol{b}_{tr}^{eT} = \boldsymbol{f}\boldsymbol{b}_n^e\boldsymbol{f}^T \tag{20}$$

The corresponding effective trial Kirchhoff stress tensor is obtained from the hyperelastic constitutive relation (5). Now the plastic function (17) is calculated using the trial Kirchhoff stress tensor and the value of the plastic multiplier from the previous time step. If the yield function is negative, the step is indeed elastic and the trial values of the quantities are the solution. On the other hand, if the yield criterion is not fulfilled and $F_p > 0$ the state is inadmissible and a plastic correction should be performed. The return mapping is performed which requires a solution of a nonlinear system of equations deduced from [2]:

$$\begin{cases} \boldsymbol{R}_\tau = \boldsymbol{b}^e(\hat{\boldsymbol{\tau}}) - \exp[-2(\gamma - \gamma_n)\boldsymbol{N}(\hat{\boldsymbol{\tau}})]\boldsymbol{b}_{tr}^e = 0 \\ R_y = F_p(\hat{\boldsymbol{\tau}}, \gamma) = 0 \end{cases} \tag{21}$$

The system (21) consists of the seven scalar equations (due to the symmetry of $\boldsymbol{b}^e$) with the seven unknowns: six components of $\boldsymbol{\tau}$ (due to the symmetry of the tensor) and γ. To find a solution of the system (21) the Newton-Raphson procedure is applied.

The next step in the algorithm is the verification of the damage condition (10) taking into account the non-local deformation measure. If the measure exceeds the previous value of the damage history parameter κ_n, then damage increases in relation to the previous time step, and a new value of the history parameter is equal to $\kappa = \bar{\epsilon}$. Otherwise, there is no damage growth and the history parameter does not change its value.

The damage variable is computed from equation (8) using the current value of the history parameter. The free energy taking into account elasticity and damage is obtained from (7).

For the uniformity of the residual vector derivation, the potential Π for the averaging differential equation (18) is applied in the algorithm. The potential originates from the weak form of the equation (18) and is assumed in such a form that $\delta\Pi = 0$ i.e.

$$\Pi(\bar{\epsilon}, \tilde{\epsilon}) = \frac{1}{2}\left[(\bar{\epsilon} - \tilde{\epsilon})^2 + l^2\nabla\bar{\epsilon}\cdot\nabla\bar{\epsilon}\right] \tag{22}$$

where the local deformation measure $\tilde{\epsilon}$ is calculated from (9). Due to the application of the potential Π, the residual vector including equilibrium and averaging equations, and the consistent tangent operator can be now calculated as follows

$$\boldsymbol{R} = \left[\frac{\partial(\psi - W^{ext})}{\partial u_1}, \frac{\partial(\psi - W^{ext})}{\partial u_2}, \ldots, \frac{\partial(\psi - W^{ext})}{\partial u_{24}}, \frac{\partial \Pi}{\partial \bar{\epsilon}_1}, \frac{\partial \Pi}{\partial \bar{\epsilon}_2}, \ldots, \frac{\partial \Pi}{\partial \bar{\epsilon}_8}\right] \quad \boldsymbol{K} = \frac{\partial \boldsymbol{R}}{\partial \boldsymbol{p}} \tag{23}$$

where $\boldsymbol{p}$ is a vector of degrees of freedom: the nodal displacements and values of non-local variable, which is the non-local deformation measure. In eq. (23) it is assumed that linear hexahedra are used for finite element interpolation of both the fields, but there is nothing against using higher-order interpolation.

It can be noticed that in the algorithm the free energy function taken into account in the residual vector does not include its plastic part. Indeed, the omitted part is used only for the derivation of the function representing hardening (13).

The summarized algorithm for the elastic-plastic-gradient-damage material model is presented in Box 1.

Given at element level:

isoparametric interpolation, current vector of nodal displacements and non-local variables: $\boldsymbol{p} = [u_1, u_2, u_3, \ldots, u_{24}, \bar{\epsilon}_1, \bar{\epsilon}_2, \ldots, \bar{\epsilon}_8]$, integration point variables at the end of previous step, i.e. deformation gradient $\boldsymbol{F}_n$, elastic left Cauchy-Green tensor $\boldsymbol{b}^e_n$, plastic strain measure γ_n, damage history parameter κ_n

Compute at each integration point:

- Relative deformation gradient: $\boldsymbol{f} = \boldsymbol{F}\boldsymbol{F}_n^{-1}$
- Trial elastic left Cauchy-Green tensor: $\boldsymbol{b}^e_{tr} = \boldsymbol{f}\boldsymbol{b}^e_n\boldsymbol{f}^T$
- Strain potential: $\psi^e(\boldsymbol{b}^e_{tr})$
- Trial effective Kirchhoff stress tensor: $\hat{\boldsymbol{\tau}}_{tr} = 2\frac{\partial \psi^e}{\partial \boldsymbol{b}^e_{tr}}\boldsymbol{b}^e_{tr}$
- Yield function for trial effective stress: $F_p(\hat{\boldsymbol{\tau}}_{tr}, \gamma_n)$
- Yield condition:
  If $F_p < 0$ then state is admissible $\rightarrow \boldsymbol{b}^e = \boldsymbol{b}^e_{tr}, \gamma = \gamma_n$
  Else if $F_p > 0$ then state is inadmissible $\rightarrow \boldsymbol{b}^e = \exp[-2\Delta\gamma \boldsymbol{N}(\hat{\boldsymbol{\tau}})]\boldsymbol{b}^e_{tr}$
  where $\hat{\boldsymbol{\tau}}$ and $\Delta\gamma$ computed from: $\begin{cases} \boldsymbol{R}_\tau = \boldsymbol{b}^e(\hat{\boldsymbol{\tau}}) - \exp[-2(\gamma - \gamma_n)\boldsymbol{N}(\hat{\boldsymbol{\tau}})]\boldsymbol{b}^e_{tr} = 0 \\ R_y = F_p(\hat{\boldsymbol{\tau}}, \gamma) = 0 \end{cases}$
- Damage loading function: $F_d(\bar{\epsilon}, \kappa)$
- Damage condition:
  If $F_d < 0$ then there is no damage growth $\rightarrow \kappa = \kappa_n$
  Else if $F_d > 0$ then damage grows $\rightarrow \kappa = \bar{\epsilon}$
- Damage variable: $\omega(\kappa) = 1 - \frac{\kappa_0}{\kappa}\left(1 - \alpha + \alpha \exp(-\beta(\kappa - \kappa_0)\right)$
- Free energy: $\psi(\boldsymbol{b}^e, \omega, \gamma) = (1 - \omega)\psi^e(\boldsymbol{b}^e)$
- Local strain measure: $\tilde{\epsilon} = \det(\boldsymbol{F}) - 1$
- Potential for averaging equation: $\Pi(\bar{\epsilon}, \tilde{\epsilon}) = \frac{1}{2}\left((\bar{\epsilon} - \tilde{\epsilon})^2 + l^2 \nabla\bar{\epsilon} \cdot \nabla\bar{\epsilon}\right)$
- Contribution to residual vector and tangent matrix for final values of $\boldsymbol{b}^e$, γ and κ:
  $\boldsymbol{R} = \left[\frac{\partial(\psi - W^{ext})}{\partial u_1}, \frac{\partial(\psi - W^{ext})}{\partial u_2}, \ldots, \frac{\partial(\psi - W^{ext})}{\partial u_{24}}, \frac{\partial \Pi}{\partial \bar{\epsilon}_1}, \frac{\partial \Pi}{\partial \bar{\epsilon}_2}, \ldots, \frac{\partial \Pi}{\partial \bar{\epsilon}_8}\right]$
  $\boldsymbol{K} = \frac{\partial \boldsymbol{R}}{\partial \boldsymbol{p}}$

Box 1. Finite element algorithm for large strain elasto-plasticity coupled with gradient damage

5 ACEGEN IMPLEMENTATION AND NUMERICAL SIMULATIONS

In order to assess the performance of the material model described above, selected results of numerical simulations are presented. The computational tests were performed using Mathematica-based programs AceGen and AceFEM [4]. The former is a multi-language numerical code generator which combines symbolic and algebraic capabilities of Mathematica, automatic differentiation technique and simultaneous optimization of expressions. The latter is a finite element engine which can be substituted by a different code like ABAQUS or FEAP. Owing to the use of AceGen the analyst can focus on the examination of alternative formulations, departing from thermodynamic potentials, and on alternative algorithmic setups.

In order to implement a material model using package AceGen, an algorithm for calculation of the contribution to residual vector and tangent matrix at each integration point of element should be written in special meta-language. This approach allows one to avoid the cumbersome derivation of the consistent tangent for the Newton-Raphson method since the derivatives in eq. (23) are computed by evoking automatic differentiation routines [4].

In the following computational tests three-dimensional, hexahedral, displacement-based, isoparametric finite elements are applied. The applied elements have standard topology and similar linear interpolation of the two fundamental unknown fields: displacements and averaged measure.

5.1 Elastic coupled to gradient enhanced damage model

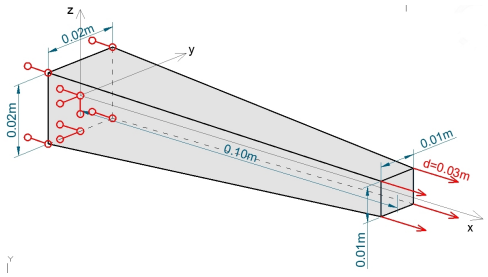

Figure 2: Geometry and boundary conditions for variable cross-section bar test

In this section the results of tests performed for the elastic-damage model with gradient averaging are presented. All simulations are performed for a bar with variable cross-section along the length. The bar is supported at one end and loaded with controlled displacement at the other. The supports are defined in such a way that uniaxial stress state is kept during deformation. The dimensions and boundary conditions are depicted in Figure 2.

The material parameters assumed in the simulations are as follows: Young modulus $E = 200\mathrm{GPa}$, Poisson ratio $\nu = 0.3$, damage threshold $\kappa_0 = 0.04$, parameters for exponential damage evolution law $\alpha = 0.95$, $\beta = 5$.

Firstly, the simulations of spatial and material averaging for three discretizations of the specimen (Figure 3) and the same material parameters are considered. The internal length for both descriptions is $l = 0.01\mathrm{m}$.

The diagrams presenting the sum of reactions on the supported end of the sample versus the displacement imposed at the other end are shown in Figure 4.

Although the simulations were performed with identical material parameters, the response for the two types of averaging differ significantly. Firstly, it can be observed that the post-peak

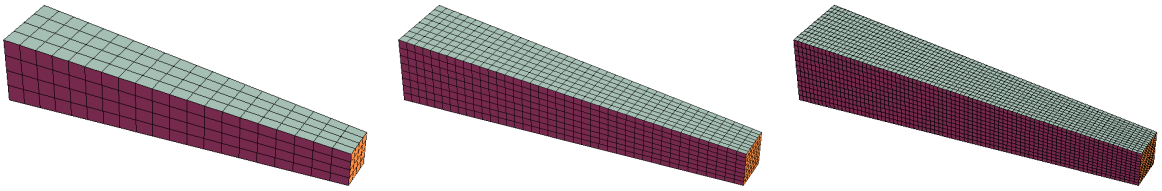

Figure 3: Discretizations of the variable cross-section bar: 20x4x4, 40x8x8, 80x12x12

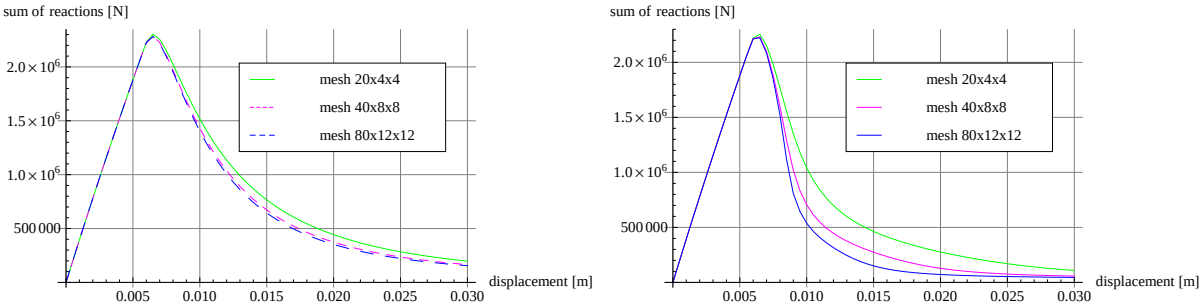

Figure 4: Displacement vs reaction sum for material and spatial averaging and different discretizations

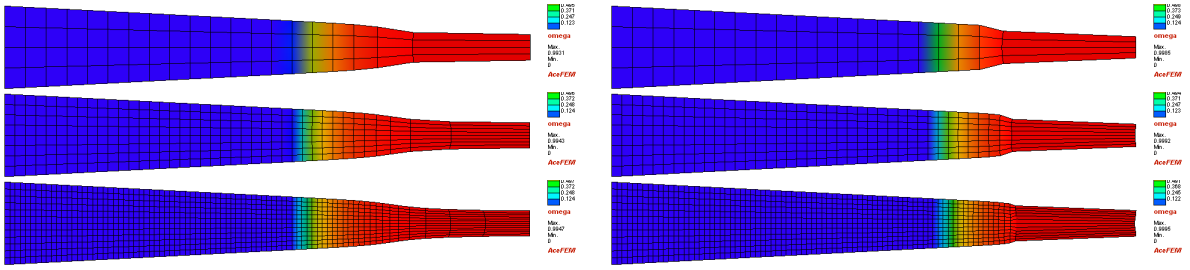

Figure 5: Deformed meshes at the end of tension test with damage variable ω distribution for material averaging (on the left) and spatial averaging (on the right)

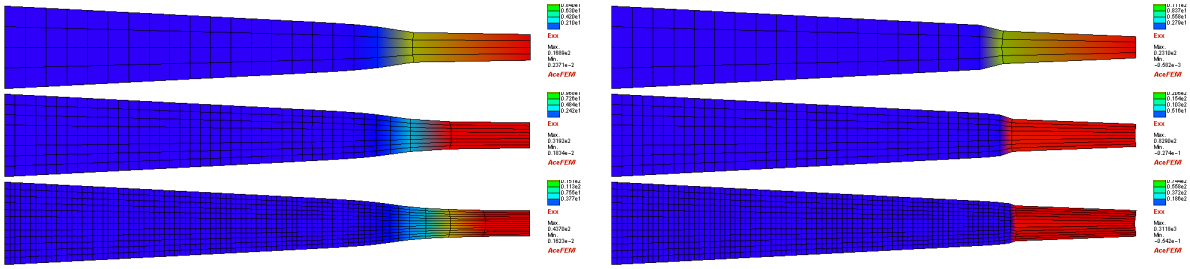

Figure 6: Deformed meshes at the end of tension test with E_{xx} distribution for material averaging (on the left) and spatial averaging (on the right)

branch for the model with spatial averaging descends more rapidly than for material averaging. Secondly, the application of spatial averaging does not result in mesh-insensitivity: for each discretization reaction diagram is different. The results for material averaging for all analyzed discretizations are close, and the diagrams for the second and the third mesh almost coincide.

It is shown in Figures 5 and 6 how the specimen deforms and the first component of the Green

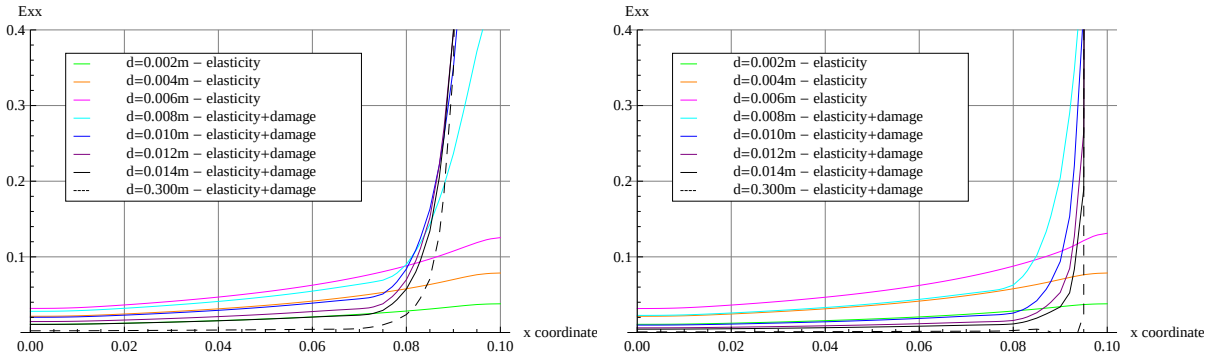

Figure 7: Evolution of the first component of Green strain tensor E_{xx} for material (on the left) and spatial (on the right) averaging - medium mesh

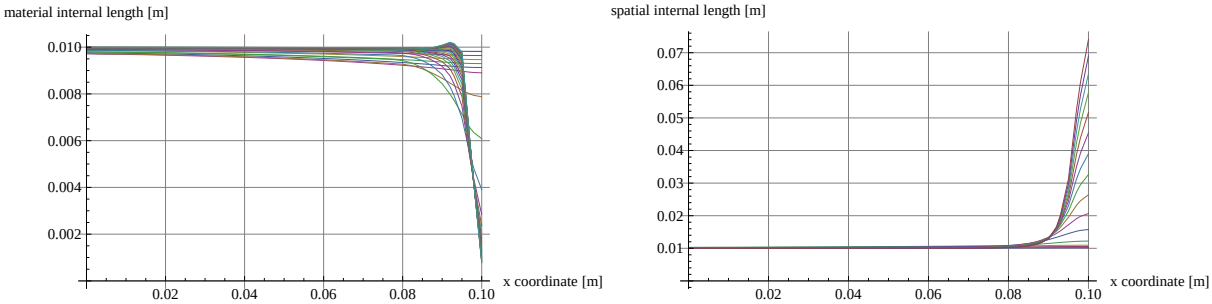

Figure 8: Evolution of material internal length whereas spatial is fixed and conversely

strain tensor E_{xx} and damage variable ω are distributed. Moreover, in Figure 7 the evolution of E_{xx} along the bar length is depicted.

It can be observed that for spatial averaging the deformation and the strain distribution depend on the finite element discretization, whereas for material averaging the response is similar for different meshes. It can be noticed in Figure 7 that as the enforced displacement increases the strain localization zone gets narrower for spatial averaging. For large enough deformation, strains concentrate in one row of elements for all analyzed discretizations. Although in the considered description the gradient regularization is applied, it does not fully preserve numerical simulations from the pathological mesh-sensitivity.

It can be noticed in Figure 5 that the damage zone is similar for all discretizations for spatial averaging although deformation differs significantly. The phenomenon is caused by irreversibility of the state of material damage. The damage area which arises at the beginning of the loading process does not decrease even if deformations concentrate in the gradually smaller band and the rest of the sample is unloaded.

The ratio of element dimension and internal length for material averaging does not change during deformation, whereas spatial averaging is performed in the current configuration thus the deformed mesh is used for the calculation of gradients. A probable explanation of the mesh-sensitivity for spatial averaging is that during deformation the dimensions of elements change whereas the internal length is assumed to be constant. This aspect of spatial averaging was also raised in the paper of Steinmann [8], who concluded from his numerical experiments that only material averaging has all desirable features to reproduce the behaviour of elastic-damaging material.

In Figure 8 the evolution of the internal length parameter along the bar for the medium mesh is presented. In the first graph we can observe the evolution of the material internal length whereas the spatial one is fixed. The value of the length parameter decreases in the damage zone with the increasing loading. On the other hand, if the material internal length is fixed, the value of the spatial one grows at the end of the bar with smaller cross-sectional area.

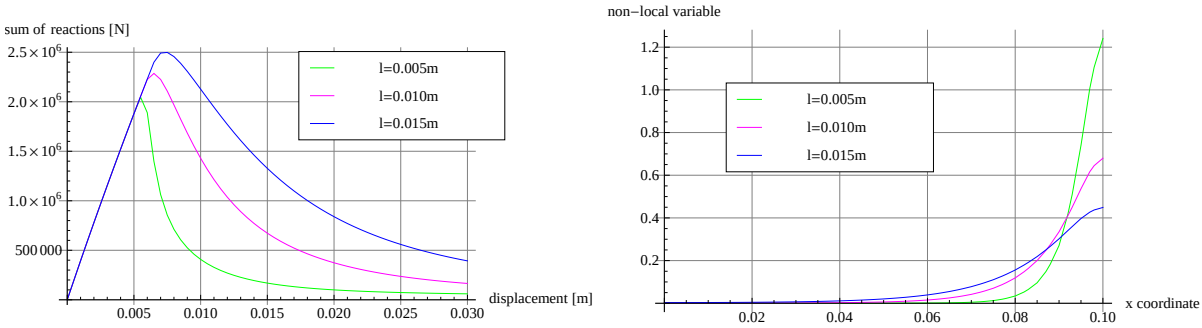

Figure 9: Displacement vs reaction sum and non-local variable distribution along the length for different values of internal length parameter

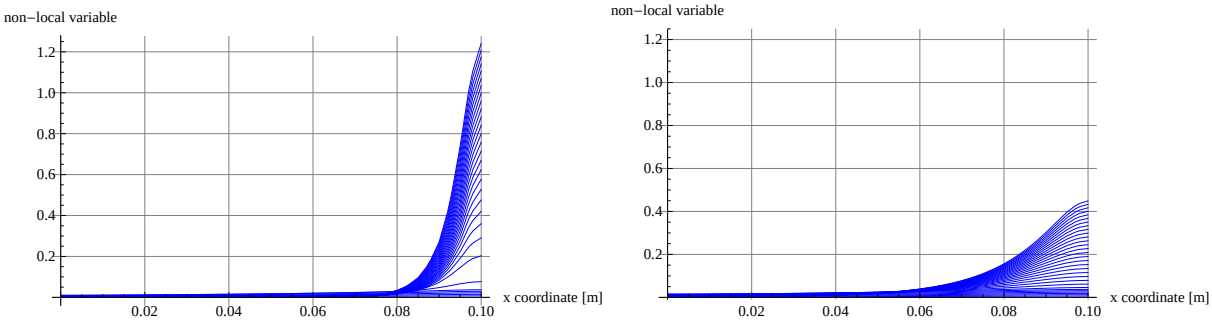

Figure 10: Evolution of non-local variable for internal lengths: $l = 0.005\mathrm{m}$ and $l = 0.015\mathrm{m}$

Taking the observations from this test into account, the following numerical simulations are performed only for the model including material averaging.

In the next test, the comparison of the material behaviour for different internal length parameter is carried out. In the simulation the medium mesh is concerned and three values of internal length were taken into account: $l = 0.005\mathrm{m}$, $l = 0.010\mathrm{m}$, $l = 0.015\mathrm{m}$. In Figures 9 and 10 the results obtained for this test are plotted. As expected, the larger is internal length parameter is, the later the damage state is reached in the specimen and the more ductile the diagram in the post-peak regime is. Figure 10 presents the evolution of the non-local deformation measure along the bar for $l = 0.005\mathrm{m}$ and $l = 0.015\mathrm{m}$.

5.2 Elastic-plastic-gradient-damage model

In this chapter the results for the material model which includes elasticity-plasticity coupled with gradient damage are presented. Firstly, the model is tested using the variable cross-section bar, then a perforated plate in tension is taken into account.

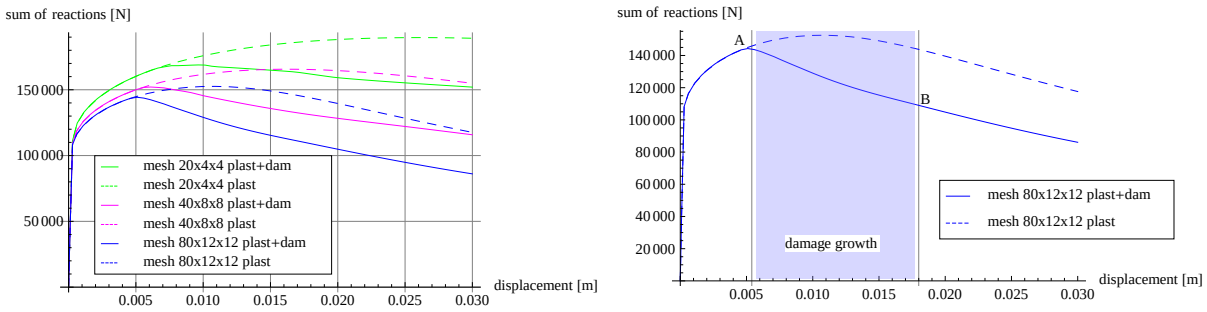

Figure 11: Displacement vs sum of reactions for variable cross-section bar - comparison of results for pure plasticity and coupled model

The geometry of the variable cross-section bar is the same as for the gradient-damage test, however the bar is fully restrained at one end. The material parameters are as in Sect. 5.1 apart from the damage threshold which now is assumed to be $\kappa = 0.003$. Additional parameters related to plasticity are: initial yield stress for tension and compression: $\sigma_{y0} = 1.225\text{GPa}$, hardening modulus: $h = 1\%E$. The test is performed for internal length scale $l = 0.01m$. The material parameters are chosen in such a way that plasticity occurs first. The relations between the enforced displacement and the sum of reactions for all considered discretizations are presented in Figure 11.

The dashed diagrams in Figure 11 present the results of the test performed for the elastic-plastic material, i.e. the damage threshold is not exceeded during the deformation process. It can be observed that for different discretizations the diagrams vary starting from the beginning of a plastic regime. This might be caused by locking problems, since the standard H1 finite elements with the first order approximation are used in the analysis.

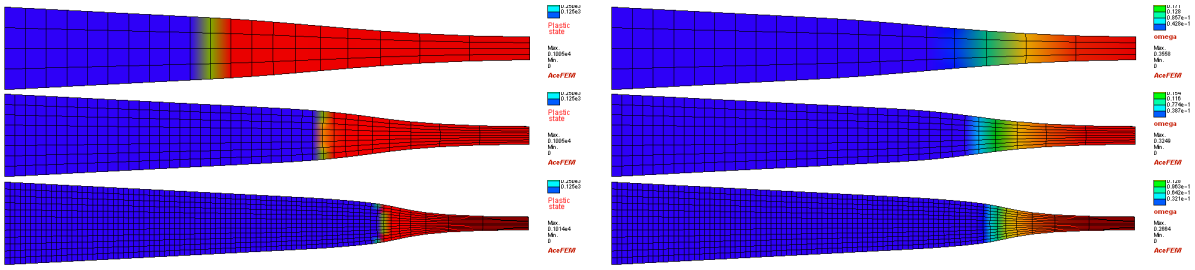

Figure 12: Deformed meshes at the end of tension test with plastic state (on the left) and damage variable ω distribution (on the right)

Although hardening of the material is assumed, softening caused by geometrical effects (necking) for the medium and the fine mesh is noticed. The area of the sample which exhibits plasticity is presented in Figure 12 on the left. The finer finite element mesh is considered, the smaller part of the sample enters the plastic state and the deformation concentrates in a narrower zone.

Taking the damage into account the reaction diagrams (solid diagrams in Figure 11) change in the relation to the plastic model. Instead of hardening, an immediate stiffness reduction occurs in the sample. For the assumed material parameters, the damage growth occurs only in a limited interval of the loading process which is shaded in the Figure 11 on the right (results for

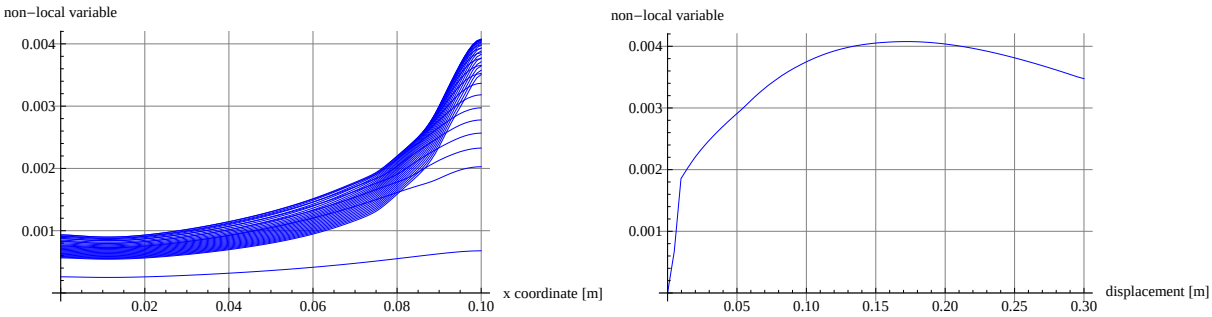

Figure 13: Evolution of non-local variable along the bar length and for the point at the loaded end for elasticity-plasticity coupled with damage (fine mesh)

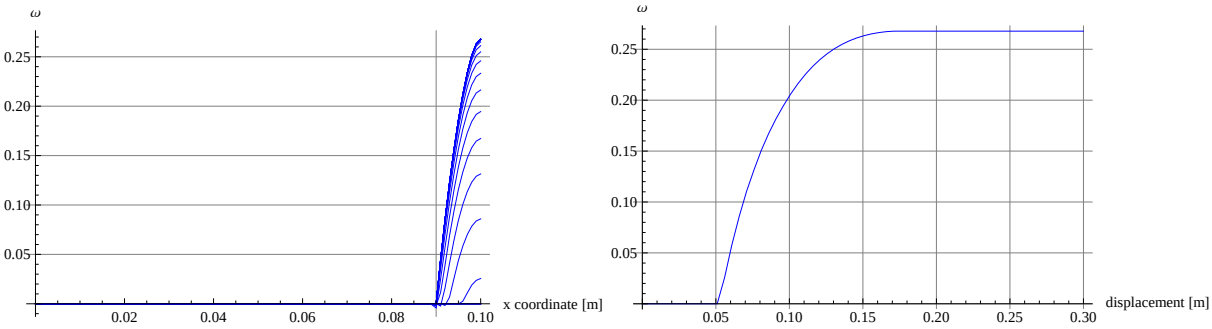

Figure 14: Evolution of the damage variable ω along the bar length and for the point at the loaded end for elasticity-plasticity coupled with damage (fine mesh)

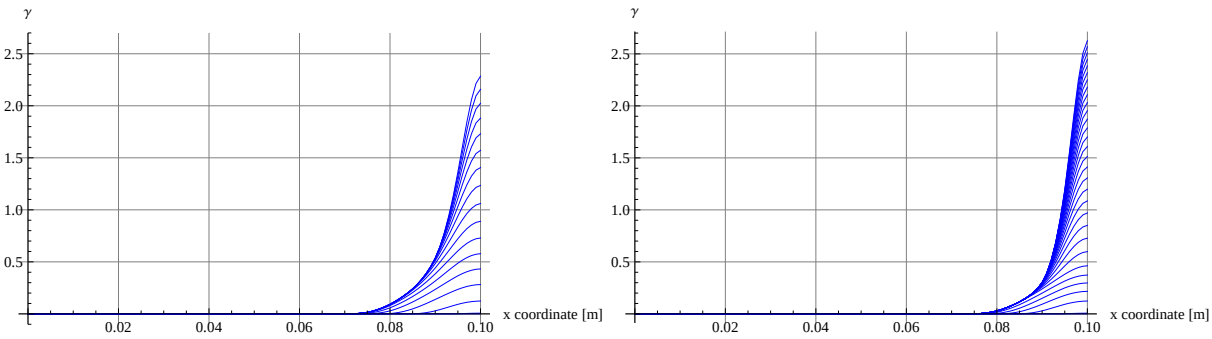

Figure 15: Evolution of the plastic multiplier for elasticity-plasticity and elasticity-plasticity coupled with damage (fine mesh)

the fine mesh). From point B the assumed averaged deformation measure related to the change of the volume ceases to increase (Figure 13), thus there is no damage growth and the damage variable ω is fixed (Figure 14). The descending branch is now caused only by geometrical softening in the plastic regime.

Figure 15 presents the results of simulations performed for the fine mesh, i.e. 80x12x12 elements. The effect of damage incorporation into the elastic-plastic model can be observed. Particularly, for the model including damage the plastic multiplier which represents the amount of plastic flow attains slightly larger values at the narrowest end of the sample, whereas the plastic zone is slightly narrower.

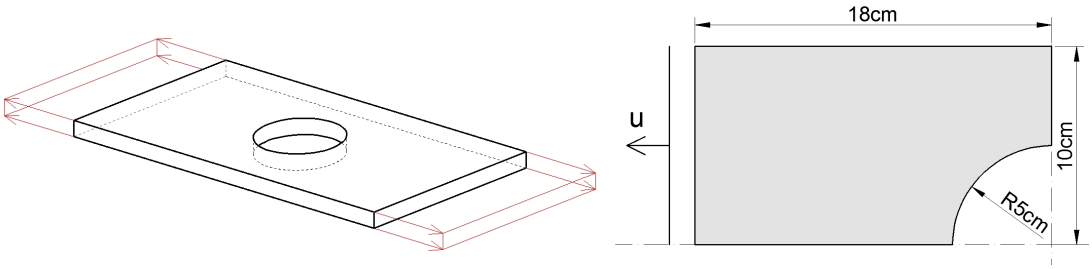

Figure 16: Geometry of perforated plate

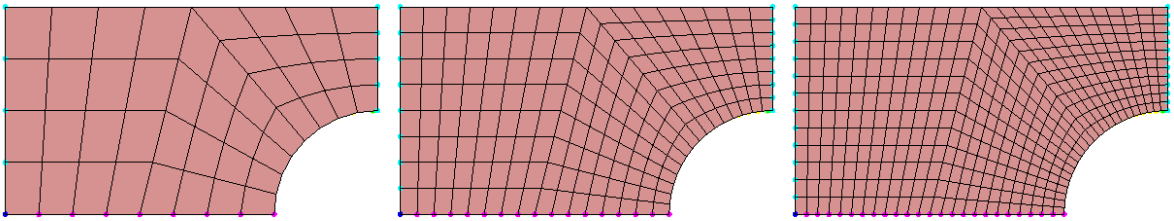

Figure 17: Discretizations of the perforated plate in tension:48 elements, 192 elements and 432 elements

The following simulations are performed for the perforated plate in tension shown in Figure 16. Due to double symmetry of the specimen, only one quarter of the perforated plate is considered. Similarly to the bar example, three discretizations are taken into account (Figure 17).

The material data are adopted as in previous test apart from the internal length parameter which now is assumed to be $l = 0.02\mathrm{m}$. The maximum displacement enforced at one end of the sample is equal to $d = 0.05\mathrm{m}$.

In Figure 18 the reaction diagrams for the considered cases are presented. In this test the mesh-sensitivity is not so pronounced in the graph as it is for the variable cross-section bar in tension, however, the differences in results are noticed in the interval of damage growth.

In Figures 19, 20 and 21 the deformed meshes and the distribution of chosen quantities are presented. Similarly to the previous test, the area of the sample which exhibits plasticity differs depending on the discretization (upper plots in Figure 19) and the finer the mesh is taken into account the more concentrated the strain becomes in the process zone. It can also be noticed that the maximum tensile stress does not concentrate at the narrowest part of the sample, but at a certain distance from the vertical axis of symmetry (Figure 21).

6 CONCLUSIONS AND FUTURE WORK

In the paper the framework of the gradient-enhanced large-strain elasticity-damage-plasticity model has been outlined. The model is based on the multiplicative decomposition of the deformation gradient (1), the Helmholtz free energy in the form (3) and is limited to isotropy and isothermal conditions. The gradient averaging is applied to the deformation measure which determines the damage growth. The numerical simulations are performed using packages AceGen/AceFEM and owing to this the consistent tangent matrix for the system of nonlinear equations is evaluated automatically.

The selected results of the computational tests for the gradient elasticity-damage and the gradient elasticity-damage-plasticity have been presented. For the former model attention is fo-

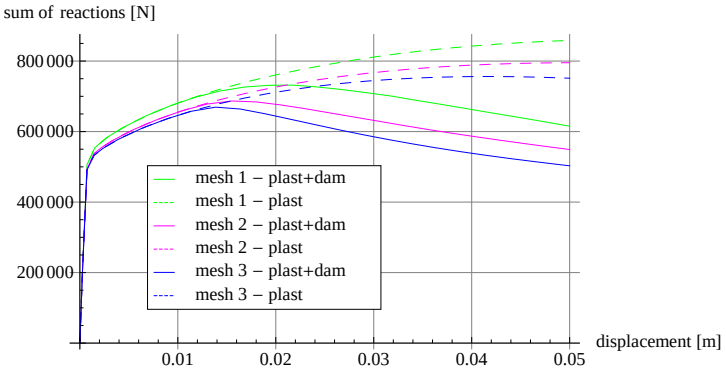

Figure 18: Displacement vs sum of reactions for perforated plate in tension

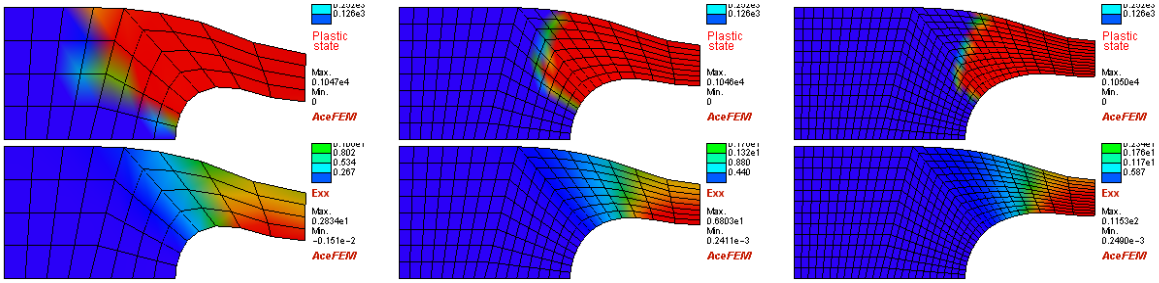

Figure 19: Deformed meshes at the end of tension test with plastic state (at the top) and E_{xx} distribution (at the bottom)

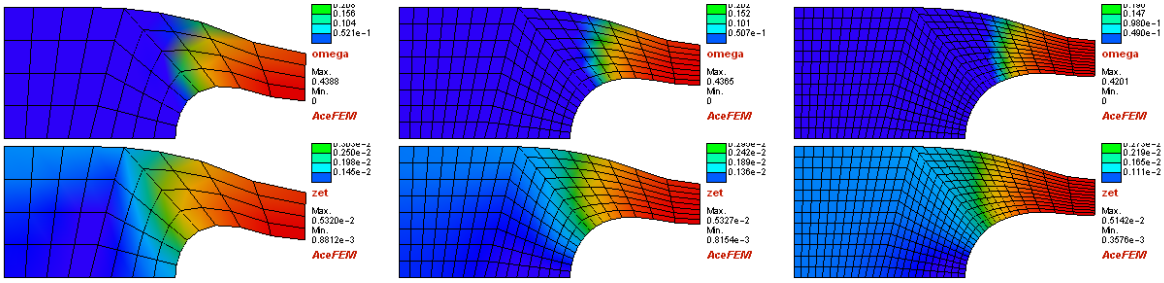

Figure 20: Deformed mesh at the end of tension test with damage variable ω (at the top) and non-local variable distribution (at the bottom)

cused on the comparison of spatial and material description. The numerical simulations reveal that spatial averaging does not fully preserve the solution from the pathological mesh-sensitivity encountered in the damage tests. For this reason the remaining simulations are performed only for material averaging. The results for the elastic-plastic-gradient-damage model are also presented. The simulations of the variable cross-section bar and the perforated plate in tension show complex nonlinear deformation states which include not only softening due to damage phenomenon but also necking.

In the subsequent research the simulations with other finite elements which are capable of reproducing the plastic behaviour without locking are planned. The application of other deformation or energy measure to govern damage should also be considered as not only the volumet-

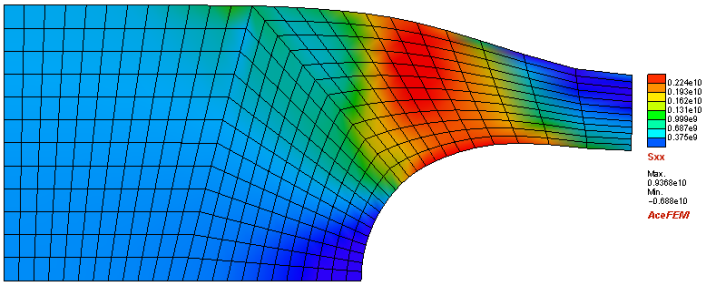

Figure 21: Cauchy stress σ_{xx} distribution in perforated plate

ric measure, as assumed in the paper in eq. (9), can be taken into account. Further, the research is going to be extended towards thermo-mechanical coupling.

REFERENCES

[1] P.M.A. Areias, J.M.A.C. de Sa, C.A.C. Antonio: A gradient model for finite strain elasto-plasticity coupled with damage. *Finite Elements in Analysis and Design*, 39 (2003), 1191–1235.

[2] F. Auricchio, R.L. Taylor: A return-map algorithm for general associative isotropic elasto-plastic materials in large deformation regimes. *International Journal of Plasticity*, 15 (1999), 1359–1378.

[3] M.G.D. Geers: Finite strain logarithmic hyperelasto-plasticity with softening: a strongly non-local implicit gradient framework. *Computer Methods in Applied Mechanics and Engineering*, 193 (2004), 3377–3401.

[4] J. Korelc: Automation of primal and sensitivity analysis of transient coupled problems. *Computational Mechanics*, 44 (2009), 631–649.

[5] K. Kowalczyk-Gajewska, J. Pamin and T. Żebro: Development of gradient-enhanced damage-plasticity formulations for large deformations. *Technical Transactions*, 20 (2008), Series Environmental Engineering 3/2008, 47–58.

[6] R.H.J. Peerlings, R. de Borst, W.A.M. Brekelmans, J.H.P. de Vree: Gradient-enhancement damage for quasi-brittle materials. *International Journal for Numerical Methods in Engineering*, 39 (1996), 3391–3403.

[7] J.C. Simo, T.J.R. Hughes: *Computational inelasticity*. Springer, 1998

[8] P. Steinmann: Formulation and computation of non-linear gradient damage. *International Journal for Numerical Methods in Engineering*, 46 (1999), 757–779.